Article ID: 1006-8775(2019) 01-0024-10

THE IMPACT OF HORIZONTAL RESOLUTION ON THE INTENSITY AND MICROSTRUCTURE OF SUPER TYPHOON USAGI

WEN Ying-fang (文映方)[1, 2], LIU Yu-di (刘宇迪)[1], TAN Wei-cai (谭伟才)[3], PENG Ke-man (彭科曼)[4], CHEN Hai-feng (陈海凤)[4]

(1. College of Meteorology and Oceanography, Defense University of Science and Technology, Nanjing 211101 China; 2. Guangzhou Meteorological Bureau, Guangzhou 511430 China; 3. Unit No.75839 of People's Liberation Army, Guangzhou 510510 China; 4. Guiyang Meteorological Bureau, Guiyang 550001 China)

Abstract: Typhoon Usagi (1319) was simulated by using the Advanced Weather Research and Forecasting numerical model (WRF) with different horizontal resolution to understand the impact of horizontal resolution on the intensity and characteristics of typhoon's microstructures (including dynamic and microphysical structure). The simulated results show that the improvement of horizontal resolution from 5 km to 1 km has little impact on the track which is comparable to real results, but has a significant impact on the intensity and microstructures, and especially, the impact on wind speed at 10 m height, the vertical movement and precipitation intensity is the greatest. When the resolution is increased to 1 km, the intensity and characteristics of typhoon's microstructures can be simulated better. In lower resolution simulations, some structural characteristics, including more asymmetrical and more outward tilted eyewall, and less water vapor flux on sea surface, work together to weaken typhoon intensity.

Key words: typhoon; horizontal resolution ; microstructure ; Usagi ; numerical simulation

CLC number: P444 **Document code:** A

doi: 10.16555/j.1006-8775.2019.01.003

1 INTRODUCTION

Much attention has been focused on the influence of the horizontal resolution of a weather simulation model on the simulation outcomes. Weisman et al. simulated squall lines using models with different horizontal resolutions (1-12 km), and discovered that mesoscale circulation and convective structure of the squall line varied significantly in different horizontal resolutions [1]. There was a delay in convection occurrence time when a coarse mesh was used because it failed to adequately simulate the non-hydrostatic process. They concluded that a 4 km resolution was sufficient to simulate the main characteristics of the squall line. Deng et al. studied models with different horizontal resolutions (45, 30, 20, and 10 km) in simulating rainstorms in the Huaihe River Basin[2]. Horizontal resolution had a great influence on the simulation of precipitation. Enhancing the horizontal resolution of the model improved the forecasting results. However, the precipitation intensity simulated by a high-resolution model was high and had a large false forecast rate. Different resolutions had little effect on the simulation effect of circulation. Zhang et al. simulated the weather development process in the agro-pastoral transitional zone of Naiman Banner, Inner Mongolia, China, using the mesoscale numerical model Advanced Regional Prediction System (ARPS) and found that enhancing horizontal resolution can recapitulate the multiscale features of atmospheric motion [3]. Davis et al. simulated hurricanes using the WRF model and found that the minimum sea-level pressure changed by 20 hPa and maximum wind speed increased by 13 m/s when the horizontal resolution changed from 4 km to 1.3 km [4]. Gentry and Lackmann used the WRF model to study the sensitivity of typhoons to horizontal grid intervals ranging from 1-8 km[5] . The central minimum air pressure declined markedly with increased resolution and large numbers of strongly ascending motion centers occurred at the eyewall when the grid interval was less than 4 km. They concluded that the grid interval used in the model should be smaller than 3 km for numerical forecasting[5]. Chen et al. and Yau et al. simulated hurricanes using the MM5 model with different horizontal resolutions [6-7]. The eyewall was wider when simulated by models with lower resolution. These studies focused on the macroscopic changes of simulation results but did not determine the influence of horizontal resolution on micro-structural (including kinetics and micro-physics) simulation. McFarquhar and Black and Rogers et al. conducted a hurricane simulation using the horizontal model and found large differences between the simulated kinetics and micro-physical structure and observations [8-9]. They suggested that this resulted mainly from the horizontal resolution although this possibility was not verified with

Received 2017-09-14; **Revised** 2018-06-15; **Accepted** 2019-02-15

Foundation item: National Natural Science Foundation of China (41875060)

Biography: WEN Ying-fang, assistant engineer, primarily undertaking research on numerical simulation.

Corresponding author: LIU Yu-di, e-mail: udy.liu@pku.edu.cn

additional research[8-9].

To study the influence of horizontal model resolutions on the kinetics and micro-physical structure of typhoons, we conducted sensitivity tests using different horizontal resolutions. Because the intensity of the typhoon center and the precipitation are largely determined by the kinetics and micro-physical structural characteristics of the typhoon (Cheng et al.[10]; He et al.[11]), this study may provide a better simulation of typhoon intensity, precipitation, and micro-structural characteristics. The results could therefore improve the accuracy of typhoon intensity prediction.

2 CASE DESCRIPTION

Typhoon Usagi, a super Typhoon coded 1319, was formed on the ocean surface to the east of the Philippines at 18:00 UTC (Coordinated Universal Time) on September 16, 2013. It strengthened from a severe tropical storm at 01:00 UTC to a typhoon at 13:00 UTC on September 18, a strong typhoon at 04:00 UTC on September 19, and further to a super typhoon at 10:00 UTC on September 19. Subject to a subtropical ridge, it moved in a WNW direction. It reached its peak intensity at 18:00 UTC on September 19 when the minimum air pressure reached 910 hPa near the typhoon center and the migration speed was 18 km/h. In the next two days, the typhoon continued to migrate in the same direction, crossing Luzong Strait and reaching the northeast area of the South China Sea. Having been downgraded to a strong typhoon at 12:00 UTC on September 21, Usagi finally landed along the coast of Dahu Township, Haifeng County, Shanwei, Guangdong Province at 11:00 UTC on September 22. Under the influence of drier air, the storm faded rapidly into a typhoon at 16:00 UTC, a severe tropical storm at 21:00 UTC, a tropical storm at 23:00 UTC on September 22, and then to a tropical depression at 08:00 UTC the day after.

3 EXPERIMENTAL SCHEME

In this study, the non-hydrostatic mesoscale numerical model WRF V3.5.1 was used. The initial field and lateral boundary of the numerical model were obtained from final operational global analysis data (at a time interval of 6 h and a horizontal resolution of 1°×1°) from the National Centers for Environmental Prediction. Five triple-nested, bi-directional grid tests were designed. Table 1 shows that the areas of innermost grids in the five tests were the same and they moved with the typhoon. The 9-3-1 km test means a test where the horizontal resolutions of the outermost grid, the middle grid and the innermost grid were 9 km, 3 km and 1 km, respectively. Emanuel noted that latent heat flux and sensible heat flux are the major energy sources of typhoons[12]. The intensity of the secondary circulation of the typhoon is largely determined by the ventilating air in upper troposphere (about 15-18 km). Therefore, unequal-distance layering was applied in the vertical direction, with the boundary layer and troposphere encrypted. There were a total of 65 layers. Dougherty and Kimball suggested that a typhoon could be better simulated using this type of vertical layering model [13]. Molinari and Dudek indicated that the grid was able to identify cumulus convection when horizontal and vertical resolutions were smaller than 5 km[14]. Thus, the GD cumulus parameterization scheme (CPS) of the innermost grid was shut down in all of the tests (Grell and Devenyi[15]). By conducting a test using a 3 km coarse grid interval and 1 km fine grid interval, Fierro et al. found that typhoon intensity and structure simulated by the coarse grid, with and without CPS, were similar[16]. Therefore, CPS was used on the second layer of the grid in the 9-3-1 km test to ensure consistency. The other parameterization schemes of physical processes remained the same in all five tests. The micro-physical scheme, long-wave radiation scheme, short-wave radiation scheme, and boundary layer scheme were WDM6 (Lim and Hong [17]), RRTM (Mlawer et al.[18]), Dudhia's model[19], and YSU (Hong et al.[20]), respectively. The simulated typhoon time was between 18:00 UTC on September 19 and 12:00 UTC on September 21, 2013 (42 h), during which the typhoon was in the maturity stage.

Table 1. Dimensions of the domains for the five tests.

Tests	Domain1	Domain2	Domian3
9-3-1km	596×496	421×301	454×454
18-6-2km	299×249	208×157	226×226
27-9-3km	199×166	142×103	151×151
36-12-4km	150×125	106×76	115×115
45-15-5km	120×100	85×61	91×91

4 SIMULATION RESULTS

Observation data of the track and intensity of typhoon used in this study was collected from the optimal track dataset for tropical cyclones developed by the China Meteorological Administration Shanghai Typhoon Institute (Ying et al.[21]). The precipitation rate was from the 2A12 dataset of the tropical rainfall measuring mission.

4.1 *Tracks*

The tracks of all five tests during the simulation were similar (Fig. 1), suggesting that the horizontal resolution had minor influence on the track of the typhoon. The similarity of simulated and observed tracks suggested that the grids in these tests were able to identify large-scale weather systems that determine typhoon tracks (Goerss[22]). However, the simulated tracks in all five tests migrated southward compared with the measured tracks during the entire simulation process, especially from 06:00 UTC to 12:00 UTC on September 21. This occurred because the subtropical high simulated in the tests was slightly high. In general, typhoon tracks were accurately simulated in all five tests and this indicated

that the environment field was accurately simulated in the tests. Differences in horizontal resolution were embodied in the simulation of typhoon intensity and micro-structure. Therefore, it was more conducive to analyzing typhoon intensity and micro-structure than analyzing typhoon track.

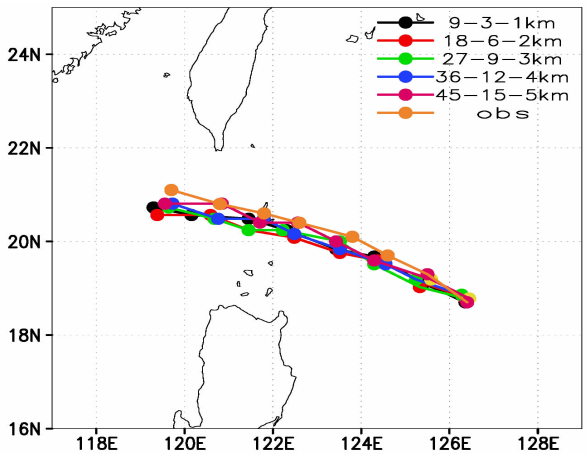

Figure 1. The typhoon tracks of five tests and the measured track from 18:00 UTC on September 19 to 12:00 UTC on September 21. The time interval is 6 hours.

4.2 *Minimum sea-level pressure and 10 m maximum wind speed*

Measured and simulated values of minimum sea-level pressure at 6 h intervals are shown in Table 2. Initial values of minimum sea-level pressure in all five tests were much larger than the measured values, which resulted from the low resolution of the initial field. Except for the 27-9-3 km test where the final simulated minimum sea-level pressure was about 9 hPa lower than the measured value, the remainder of the tests accurately simulated the minimum sea-level pressure of the typhoon from 00:00 UTC of September 21. The simulation effect of the 9-3-1 km test was better than that of any other tests. The maximum difference between minimum sea-level pressure values, simulated by various tests, was about 5 hPa throughout the entire simulation, which was different from the simulation result obtained by Davis et al.[4]. A 20 hPa decline of minimum sea-level pressure was observed using the WRF model as the horizontal resolution increased from 4 km to 1.3 km. This might have been caused by selection bias.

In all five tests, the initial 10 m maximum wind speed (MWS) was much smaller than the measured value. The 10 m MWS was accurately simulated by the 9-3-1 km test from 06:00 UTC on September 20, which was much earlier than the other tests (Fig. 2). The difference between the 10 m MWS simulated by the 9-3-1 km test and the measured value was 2.7 m/s, whereas this difference was > 7 m/s in all other tests. The 10 m MWS simulated by the 36-12-4 km test rose by 7.8 m/s from 12:00 UTC on September 20 to 00:00 UTC on September 21, during which the 10 m MWS values varied little in the other tests. Simulation effects of tests with higher resolutions were better than those of tests with lower resolutions. The measured 10 m MWS declined and dropped by 5.6 m/s from 00:00 UTC to 12:00 UTC on September 21. During the same period of time, 10 m MWS values of the 9-3-1 km test and the 36-12-4 km test showed the same trend of change as the measured value and declined by 5.6 m/s and 6.5 m/s, respectively. The 10 m MWS of the 18-6-2 km test and the 27-9-3 km test increased by 7.6 m/s and 7.2 m/s, respectively. The 10 m MWS of the 45-15-5 km test declined after an initial increase. These results indicate that the simulation effects of 10 m MWS differed greatly when using different horizontal resolutions. The 10 m MWS simulated with a higher resolution was larger than that with a smaller resolution. The simulation of 10 m MWS at a 1 km resolution was the most accurate.

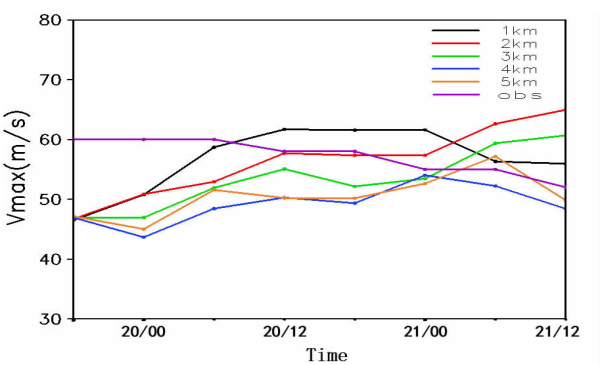

Figure 2. Time series of measured and simulated values of 10 m MWS.

Table 2. Measured and simulated values of minimum sea-level pressure (hPa).

Time (UTC)	Measured values	9-3-1km	18-6-2km	27-9-3km	36-12-4km	45-15-5km
18:00, 19th	915	964.922	964.921	965.073	965.158	964.946
00:00, 20th	915	939.542	940.089	940.536	941.052	941.820
06:00, 20th	915	931.648	933.901	934.704	935.959	935.149
12:00, 20th	920	926.155	927.085	929.632	930.944	932.141
18:00, 20th	920	927.828	926.738	926.461	927.401	930.026
00:00, 21st	925	926.535	925.139	926.343	924.100	925.129
06:00, 21st	925	925.356	922.095	922.829	922.711	921.517
12:00, 21st	930	925.599	920.865	923.428	924.501	923.444

4.3 *Precipitation*

The observed precipitation (Fig. 3f) showed two heavy precipitation areas on the southwest and southeast side of the typhoon center at 02:00 UTC on September 21. The precipitation on the southeast side was heavier and reached a maximum of 67 mm/h. The precipitation areas simulated in all five tests were similar to the observed areas (Figs.3a-3e). Differences were seen in the 36-12-4 km test and the 45-15-5 km test where heavy precipitation was concentrated on the southwest side of typhoon center. Heavy precipitation was observed on both southwest and southeast sides of the typhoon center in the rest of the tests. Simulated precipitation intensities varied with horizontal resolutions. Maximum precipitation rates in the 9-3-1 km, 18-6-2 km, 27-9-3 km, 36-12-4 km, and 45-15-5 km tests were 75 mm/h, 88 mm/h, 110 mm/h, 61 mm/h, and 70 mm/h, respectively. This indicated that precipitation intensities of 18-6-2 km test and 27-9-3 km test were larger than observed values, which could be verified by the area of precipitation larger than 50 mm/h. Moreover, the 9-3-1 km test was the only test where the heavy precipitation at the south end of Taiwan Island and north end of the Philippines, brought about by a spiral rain band, was simulated. In terms of precipitation distribution and intensity, the 9-3-1 km test was close to the actual situation.

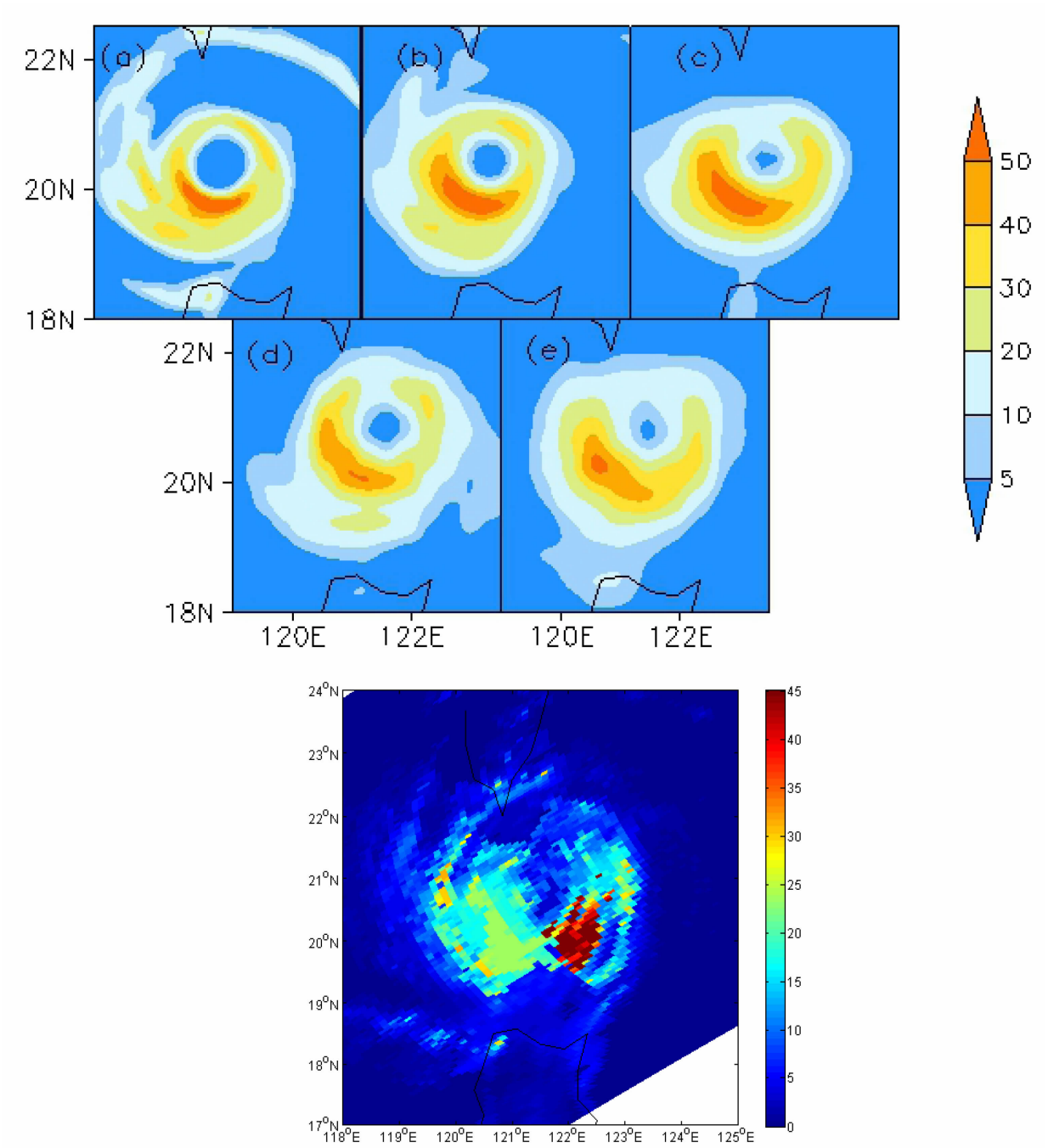

Figure 3. Measured and simulated precipitation (mm/h) at 02:00 UTC on September 21. a.9-3-1km test; b.18-6-2km test; c.27-9-3km test; d.36-12-4km test; e.45-15-5km test; f. Measured value.

4.4 *Sea surface water–vapor flux*

The sea surface water-vapor flux varied with the horizontal resolution. In the 27-9-3 km test and the 45-15-5 km test, areas with sea surface water-vapor flux larger than 0.4 g/(m^2 ·s) were small (Fig. 4). This corresponded with the small 10 m MWS values in the two tests and indicated that the typhoon intensity was largely determined by sea surface water-vapor flux. In addition, the sea surface water-vapor flux in the 45-15-5 km test showed asymmetry—the water-vapor flux on the east side of typhoon center was larger than that on the west side, which might be a primary cause of the distinct structural asymmetry of the typhoon simulated in this test.

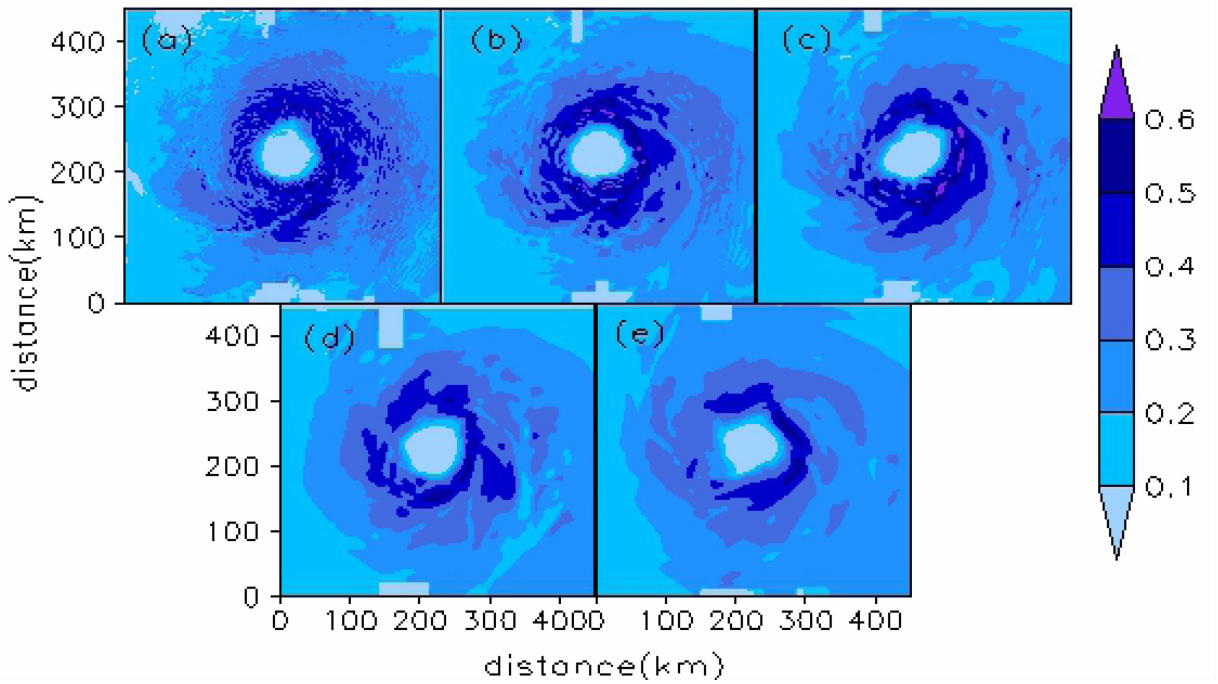

Figure 4. Simulated sea surface water-vapor flux (g/m^2· s) at 02:00 UTC on September 21. a. 9-3-1km test; b. 18-6-2km test; c. 27-9-3km test; d. 36-12-4km test; e. 45-15-5km test.

4.5 *Vertical speed*

Figure 5 (b1-b5) shows that convective characteristics at the height of 1 km varied with different resolutions. Vertical motions in the eyewall and peripheral spiral rain bands were primarily ascending motions in the 45-15-5 km test and the 36-12-4 km test. There was no noticeable sinking motion in the eye area in the 45-15-5 km test. As horizontal resolution enhanced, noticeable sinking motions occurred in the eye area and the strength of ascending motions in the eyewall and peripheral spiral rain band, along with the upward mass flux within the corresponding boundary layer (Table 3), increased. When resolution reached 1 km, a large number of strong ascending motion centers and a small number of strong descending motion occurred in the eyewall. Vertical speed range was 9-13 m/s in the eyewall, whereas it was 1-3 m/s in the 45-15-5 km test. In the presence of a small number of strong descending motions, the net mass flux in the vertical direction within the boundary layer still declined even though ascending motions were strengthened (Table 3). Maximum vertical speed in the lower layers, at the 1 km resolution, agreed with the observations of Jorgensen et al. [23], Marks and Houze[24], Black et al.[25], Eastin et al.[26], and Marks et al.[27] in the order of magnitude. Therefore, the 9-3-1 km test was close to the observed vertical speed condition.

Table 3. Upward mass flux and vertically net mass flux at 02:00 UTC on September 21 averaged in the cube whose center is the location of minimum sea-level pressure. The dimensions of the cube are respectively 300 km, 300 km, and 1.125 km.

Tests	Upward mass flux (g·m·s^{-1})	Vertical net mass flux (g·m·s^{-1})
45-15-5km	1.346	0.773
36-12-4km	1.627	0.707
27-9-3km	1.926	0.711
18-6-2km	2.705	0.739
9-3-1km	3.570	0.624

To fully describe the vertical motion characteristics of the typhoon, the simulated vertical speed was averaged along the azimuth. There were multiple large-value zones of ascending motions distributed along the vertical profile in all the tests (Fig. 6). Similar structures were also found by Black et al. [25] when they observed and simulated mature hurricanes and by Samsury and Zipser[28], May and Rajopadhyaya [29] and Fierro et al. [30] and Fierro et al. [31] when they investigated tropical ocean squall lines. They

found that large-value zones of lower-layer ascending motions were the result of dynamic friction, whereas large-value zones on upper layers resulted from water unloading and buoyancy. Vertical motions in both lower and upper layers were large in the 18-6-2 and 36-12-3 km tests, suggesting that overall intensities of ascending motions were strong in these two tests. Although the intensities of lower-layer ascending motions simulated in the 9-3-1 km test were the strongest, based on Fig. 5, the overall intensity of ascending motions was still weak since there were some strong descending motions in the lower levels simulated in this test. This was confirmed by the small net mass flux in the vertical direction on the boundary layer in the 9-3-1 km test. It also indicated that the inclination of a large-value zone of ascending motions increased with the grid interval, suggesting an increasing

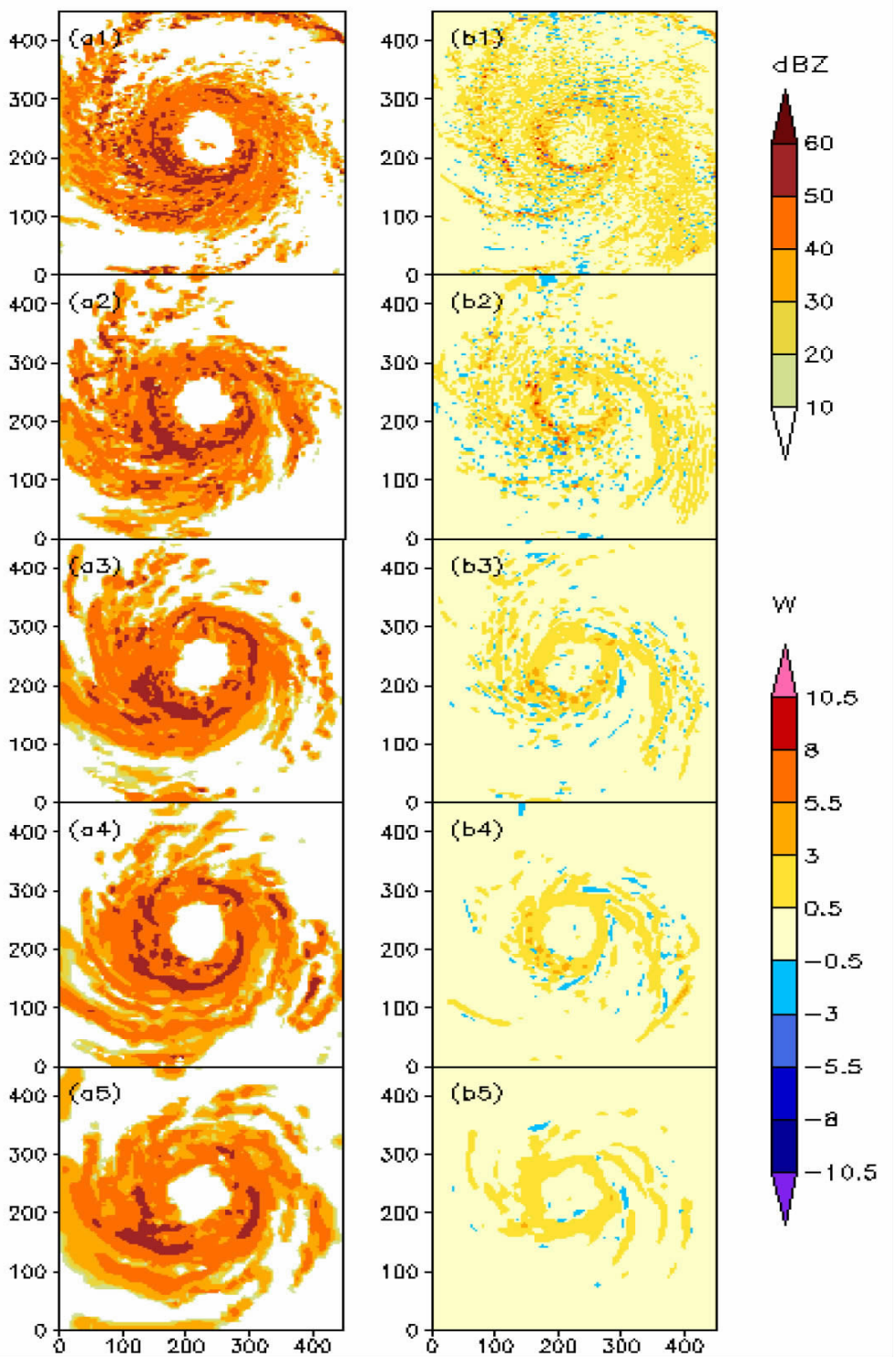

Figure 5. Simulated radar reflectivity (a1-a5, dBZ) and vertical wind speed (b1-b5, m/s) at z =1 km at 02:00 UTC on September 21. The order of the five tests is with the finest-resolution test shown at the top line and the coarsest simulation test shown at the bottom line.

eyewall inclination with grid interval. When the eyewall inclination of the typhoon was large, the heating effect with the release of latent heat of condensation within middle layers reduced the pressure gradient in the radius of maximum wind and enhanced the pressure gradient outside the radius of maximum wind, which not only weakened typhoon intensity but also enlarged the scale of the inner zone of the typhoon (Wang[32]). According to the eyewall inclination, the intensity of the typhoon simulated by the model with a low resolution was weak, which is consistent with the low 10 m MWS in low resolution tests.

4.6 *Eyewall of the typhoon*

The typhoon eyewall is the source of heavy precipitation and the intensity of the storm surge is largely determined by the range of lower-layer high wind speed. Therefore, it is important to study the eyewall structural characteristics simulated with different resolutions. The eyewall simulated by a low resolution model was wide, which was attributed to the large eyewall inclination (Fig. 5 (a1-a5)). This also suggested more prominent asymmetry of the eyewall at a low resolution. In mature typhoons, asymmetric flow would absorb kinetic energy from symmetric flow, in which tangential wind speed and radial wind speed decreases (Peng et al.[33]; Wu and Braun[34]; Yang et al. [35]). Thus, when the resolution is low, an eyewall with prominent asymmetry results in a typhoon with low wind speed.

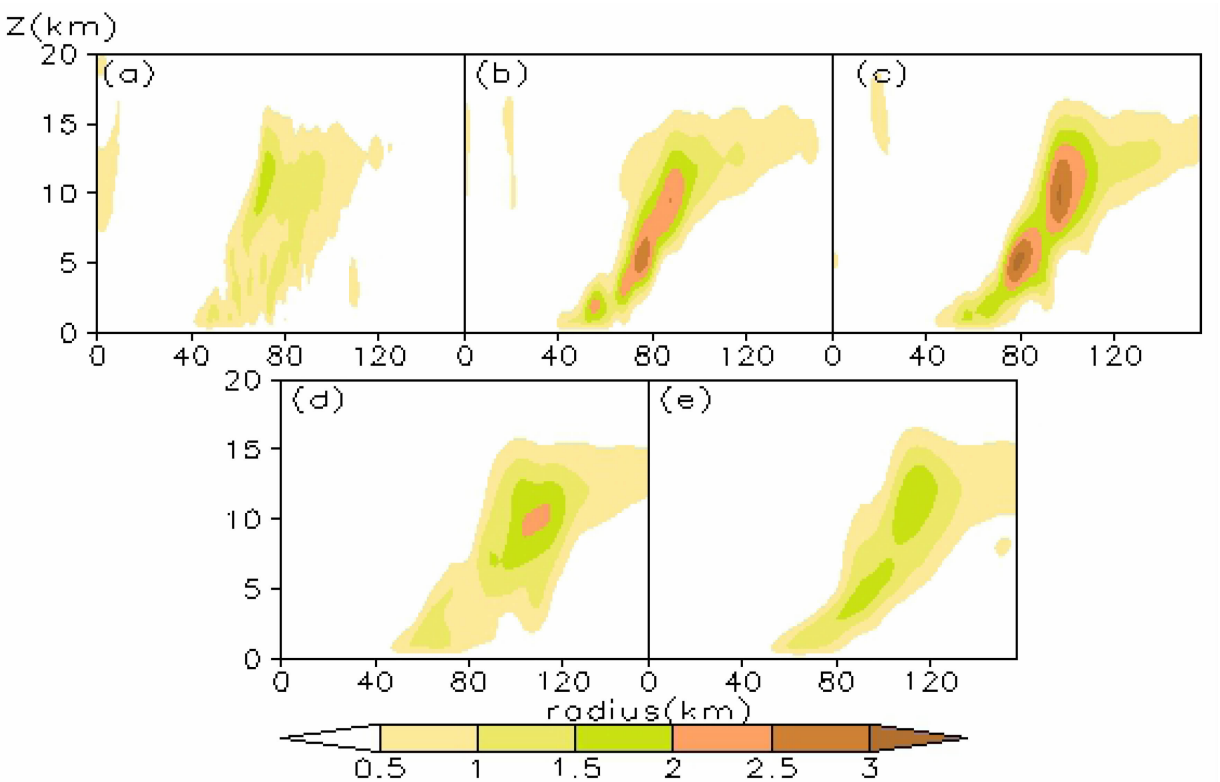

Figure 6. Height-radius plots of mean azimuthal vertical wind speed (m/s) at 02:00 UTC on September 21. a. 9-3-1 km test; b. 18-6-2 km test; c. 27-9-3 km test; d. 36-12-4 km test; e. 45-15-5 km test.

4.7 *Hydrometer distribution*

Figure 7 (a1-a5) shows that the area enclosed by the isoline where graupel content was 1.5 g/kg was the smallest in the 9-3-1 km test, in which the maximum mixing ratio of graupel was 2 g/kg. The area was the largest in the 18-6-2 km test and the 36-12-3 km test, in which the maximum mixing ratio of graupel reached 3.6 g/kg. The area enclosed by the isoline where rain water content was 2 g/kg was also the largest in the 18-6-2 km test and the 36-12-3 km test and smallest in the 9-3-1 km test. Snow content was the largest in the 27-9-3 km test and the smallest in the 45-15-5 km test. The large-value zone of snow was above that of graupel, suggesting that a large amount of graupel originated from snow. Large-value zones of rain water were below the large-value zone of graupel in all of the tests, which indicated a large amount of rain water derived from melted graupel particles. Fig. 7 (b1-b5) shows that large-value zones of cloud ice were near a height of 12 km in all the tests. Cloud ice content was the largest in the 27-9-3 km test and the smallest in the 45-15-5 km test. Large-value zones of cloud ice content were observed near the melting layer (at a height of ~5 km) and the top boundary layer. Cloud water content near the top layer of the eye area varied significantly and was largest in the 45-15-5 km test. Such a difference might be attributed to a different description of turbulence on the low-altitude frictional layer by the model at different resolutions.

In general, there was more hydrometeor simulation at the resolution of 18-6-2 km and 27-9-3 km, which

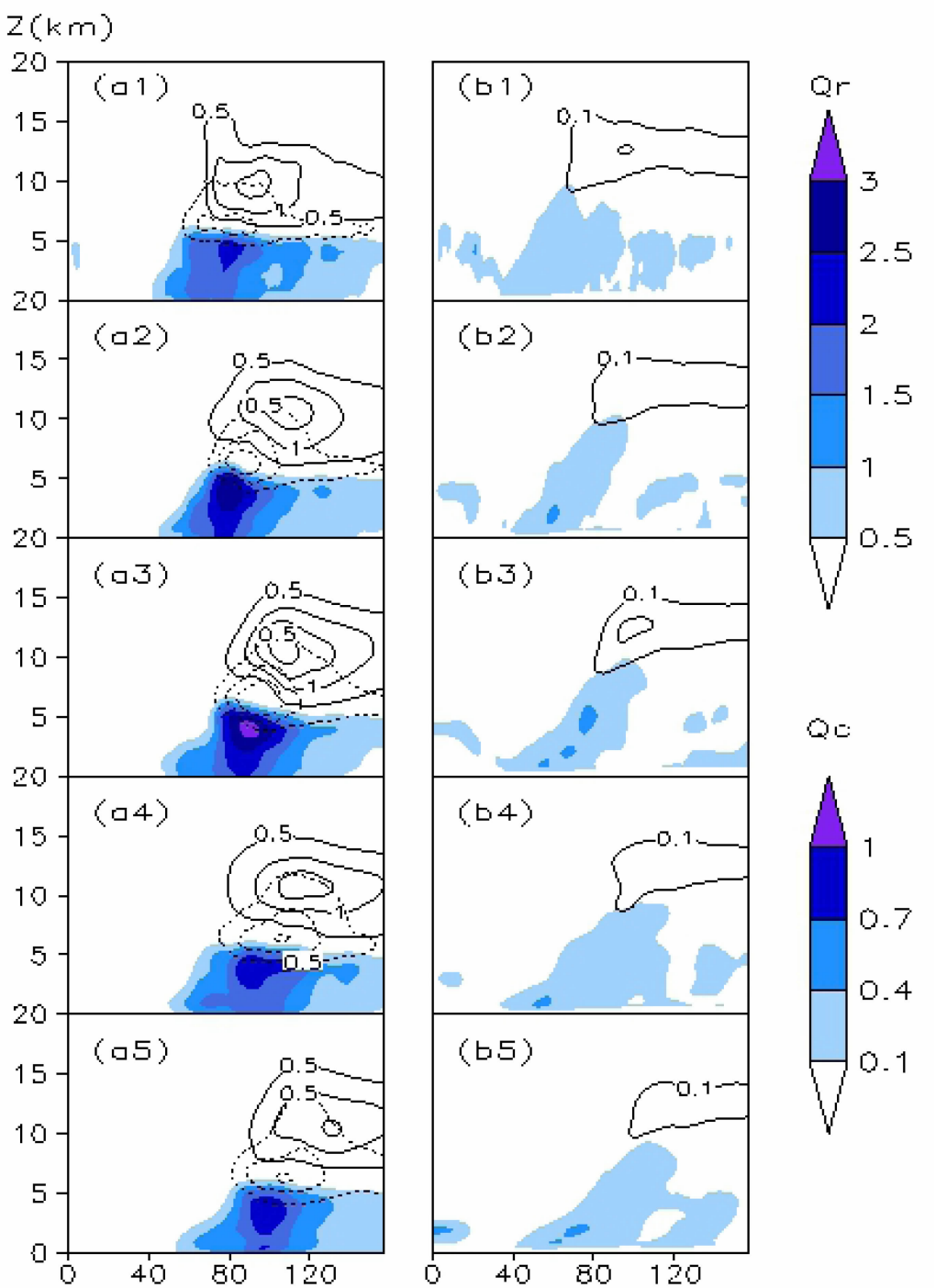

Figure 7. Height-radius plots of mean azimuthal hydrometer mixing ratio (g/kg) at 02:00 UTC on September 21. In the left column shadow shows rain (Qr) , dashed line shows graupel and solid line shows snow. In the right column shadow shows cloud water (Qc) and line shows cloud ice. The order of five tests is with the finest-resolution test shown at the top line and the coarsest simulation test shown at the bottom line.

would enhance precipitation. This was consistent with the results shown in Fig. 3. Surface precipitation intensity was high in the 18-6-2 km and 36-12-3 km tests. Ascending motions showed an overall strong intensity in both tests, suggesting that the hydrometeor contents and precipitation intensity were largely determined by the overall intensity of ascending motions. The 1 km resolution was more capable of simulating precipitation intensity than the other resolutions, which further indicated that the vertical motions simulated at the resolution of 1 km were close to actual conditions. The radius of large-value zones of graupel and snow content increased with the grid interval, suggesting that the eyewall inclination rose with grid interval. This was consistent with the conclusion that eyewall inclination was the largest in the 45-15-5 km test, which was judged

based on ascending motions.

5 DISCUSSION AND CONCLUSIONS

A mesoscale model WRF with different horizontal resolutions (1, 2, 3, 4, and 5 km) was used to simulate Typhoon Usagi. We reached the following conclusions.

(1) Horizontal resolutions do not have significant influence on the simulation effect of typhoon tracks; the model can accurately simulate typhoon tracks at various resolutions.

(2) Different horizontal resolutions show different simulation effects on typhoon intensity (defined by minimum sea-level pressure or 10 m MWS), especially for 10 m MWS. The typhoon intensity simulated at 1 km resolution was close to the observed value.

(3) Horizontal resolutions have a significant influence on the simulation effects of the microstructure of typhoons (including dynamics and micro-physics). The greatest influence was found on vertical motions and precipitation intensity. There were high precipitation intensities, high hydrometeor content, and strong overall intensity of ascending motions when the horizontal resolutions were 2 km and 3 km, indicating that the difference in the capability of different horizontal resolutions in vertical motion simulation is the major cause leading to the difference of the capability of the model in precipitation intensity simulation. A 1 km resolution showed the best precipitation intensity simulation and indicates that the vertical motions simulated at a 1 km resolution are close to actual conditions. The magnitude of lower-layer vertical motions simulated at 1 km resolution is the same as that of mass observation, verifying the previous conclusion. Increasing the horizontal resolution model to 1 km was helpful for improving the simulation effects of precipitation intensity and vertical motion.

(4) The simulated typhoon intensity is small when simulated at a low resolution, which is associated with the small water-vapor flux, asymmetry of the eyewall, and large eyewall inclination.

Previous studies reported that enhancing the horizontal resolution would contribute to the explicit description of atmospheric thermal processes and dynamic processes by the model and reduce the parameterization process (Zhang and Wei [36]; Chen and Xue [37]; Liao [38]). This might be the main reason why various factors like ascending motion and upward mass transport are large. For calculation accuracy, the smaller the grid interval, the better the numerical calculations reflect the actual climate situation. Therefore, the simulation result with 1 km horizontal resolution is superior to those with lower resolutions. However, our results are presented considering all physical processes, whereas there are interactions, including non-linear energy cascades, between these physical processes. Due to the limited space of this paper, it is difficult to conduct detailed analysis of the mechanism leading to different micro-structures here.

The conclusions of this study are based on a single case with specific physical processes. Situations with different parameters might produce different results. Thus, statistical analysis of more cases is required before reaching more general conclusions.

REFERENCES:

[1] WEISMAN M L, SKAMAROCK W C, KLEMP J B. The resolution dependence of explicitly modeled convective systems[J]. Mon Wea Rev, 1997, 125(4): 527-548.

[2] DENG Lian-tang, SHI Xue-li, YAN Zhi-hui. Mesoscale simulation of heavy rainfall in the Huaihe river valley in July 2003: Effects of different horizontal resolutions [J]. J Trop Meteor, 2012, 28(2): 167-176 (in Chinese).

[3] ZHANG Yu, GUO Zhen-hai, ZHANG Huang-yu, et al. Analysis of mesoscale numerical model's ability of atmospheric multi-scale characteristics simulation in variety resolution [J]. J Atmos Sci, 2010, 34 (3): 653-660 (in Chinese).

[4] DAVIS C, WANG W, CHEN S S, et al. Prediction of landfalling hurricanes with the Advanced Hurricane WRF Model [J]. Mon Wea Rev, 2008, 136(6): 1990-2005.

[5] GENTRY M S, LACKMANN G. Sensitivity of simulated tropical cyclone structure and intensity to horizontal resolution [J]. Mon Wea Rev, 2010, 138(3): 688-704.

[6] CHEN S S, PRICE J F, ZHAO W, et al. The CBLAST-Hurricane Program and the next generation fully coupled atmosphere- wave- ocean models for hurricane research and Prediction [J]. Bull Amer Meteor Soc, 2007, 88(3): 311-317.

[7] YAU M K, LIU Y , ZHANG D L, et al. A multiscale numerical study of Hurricane Andrew (1992), Part VI: Small scale inner-core structures and wind streaks [J]. Mon Wea Rev, 2004, 132(6): 1410-1433.

[8] McFARQUHAR G M, BLACK R A. Observations of particle size and phase in tropical cyclones: Implications for mesoscale modeling of microphysical processes [J]. J Atmos Sci, 2004, 61(4): 422-439.

[9] ROGERS R F, BLACK M L, CHEN S S, et al. An evaluation of microphysics fields from mesoscale model simulations of tropical cyclones, Part I: Comparisons with observations [J]. J Atmos Sci, 2007, 64 (6): 1811-1834.

[10] CHENG Rui, YU Ru-cong, XU You-ping, et al. Numerical research on intensity change and structure feature of Typhoon Rananim near shore: Impact of cloud microphysical parameterization on intensity and track [J]. Acta Meteor Sinica, 2009, 67 (5): 777-789 (in Chinese).

[11] HE Hui-zhong, CHENG Ming-hu, ZHOU Feng-xian. 3D structure of rain and cloud hydrometeors for Typhoon Kujira (0302) [J]. J Atmos Sci, 2006, 30(3): 491-502 (in Chinese).

[12] EMANUEL K A. An air-sea interaction theory for tropical cyclone, Part I: Steady state maintenance [J]. J Atmos Sci, 1986, 43(6): 585-604.

[13] DOUGHERTY F C, KIMBALL S K. The sensitivity of hurricane simulations to the Distribution of vertical levels in MM5 [J]. Mon Wea Rev, 2006, 134(7): 1987-2008.

[14] MOLINARI J, DUDEK M. Parameterization of convective precipitation in mesoscale numerical models: A critical review [J]. Mon Wea Rev, 1992, 120 (2):

326-344.
[15] GRELL GA, DEVENYI D. A generalized approach to parameterizing convection combining ensemble and data assimilation techniques [J]. Geophys Res Lett, 2002, 29 (14): 38-41.
[16] FIERRO A O, ROGERS R F, MARKS F D, et al. The impact of horizontal grid spacing on the microphysical and kinematic structures of strong tropical cyclones simulated with the WRF-ARW Model [J]. Mon Wea Rev, 2009, 137(11): 3717-3743.
[17] LIM K S, HONG S Y. Development of an effective double-moment cloud microphysics scheme with prognostic cloud condensation nuclei (CCN) for weather and climate models [J]. Mon Wea Rev, 2011, 138(5): 1587-1612.
[18] MLAWER E J, TAUBMAN S J, BROWN P D, et al. Radiative transfer for inhomogeneous atmosphere: RRTM, a validated correlated-k model for the longwave [J]. J Geophys Res, 1997, 102(D14): 16663-16682.
[19] DUDHIA J. Numerical study of convection observed during the winter monsoon experiment using a mesoscale two-dimensional model [J]. J Atmos Sci, 1989, 46(20): 3077-3107.
[20] HONG S Y, NONG Y, DUDHIA J. A new vertical diffusion package with an explicit treatment of entrainment processes [J]. Mon Wea Rev, 2006,134(9): 2318-2341.
[21] YING M, ZHANG W, YU H, et al. An overview of the China Meteorological Administration tropical cyclone database [J]. J Atmos Oceanic Technol, 2014, 31(2): 287-301.
[22] GOERSS J S. Prediction of tropical cyclone track forecast error for Hurricanes Katrina, Rita, and Wilma [R]. 27th Conf on Hurricanes and Tropical Meteorology, 2006, Monterey, CA, Amer Meteor Soc, 2006, 11A.1.
[23] JORGENSEN D P, ZIPSER E J, LeMONE M A. Vertical motions in intense hurricanes [J]. J Atmos Sci, 1985, 42 (8): 839-856.
[24] MARKS F D, HOUZE R A. Inner core structure of Hurricane Alicia from airborne Doppler radar observations [J]. J Atmos Sci, 1987, 44(9): 1296-1317.
[25] BLACK M L, BURPEE R W, MARKS F D. Vertical motion characteristics of tropical cyclones determined with airborne Doppler radial velocities [J]. J Atmos Sci, 1996, 53(13): 1887-1909.
[26] EASTIN M D, GRAY W M, BLACK P G. Buoyancy of convective vertical motions in the inner core of intense hurricanes, Part I: General statistics [J]. Mon Wea Rev, 2005, 133(1): 188-208.
[27] MARKS F D, BLACK P G, MONTGOMERY M T, et al. Structure of the eye and eyewall of Hurricane Hugo (1989) [J]. Mon Wea Rev, 2008, 136(4): 1237-1259.
[28] SAMSURY C E, ZIPSER E J. Secondary wind maxima in hurricanes: Airflow and relationship to rainbands [J]. Mon Wea Rev, 1995, 123(12): 3502-3517.
[29] MAY P T, RAJOPADHYAYA D K. Wind profiler observations of vertical motion and precipitation microphysics of a tropical squall line [J]. Mon Wea Rev, 1991,124(4): 621-633.
[30] FIERRO A O, LESLIE L M , MANSELL E R, et al. Numerical simulations of the electrification and microphysics of the weakly electrified 9th February 1993 TOGA COARE squall line, 2008: Comparisons with observations [J]. Mon Wea Rev, 2008, 136(1): 364-379.
[31] FIERRO A O, SIMPSON J, LeMONE M A, et al. On how hot towers fuel the Hadley cell: An observational and modeling study of line-organized convection in the equatorial trough from TOGACOARE [J]. J Atmos Sci, 2009, 66(9): 2730-2746.
[32] WANG Y. How do outer spiral rainbands affect tropical cyclone structure and intensity [J]. J Atmos Sci, 2009, 66: 1250-1273.
[33] PENG M S, JENG B F, WILLIAMS R T. A numerical study on tropical cyclone Intensification, Part I: Beta effect and mean flow effect [J]. J Atmos Sci, 1991, 56 (10): 1404-1423.
[34] WU L, BRAUN S A. Effects of environmentally induced asymmetries on hurricane intensity: A numerical study [J]. J Atmos Sci, 2004, 61(24): 3065-3081.
[35] YANG B, WANG Y, WANG B. The effect of internally generated inner-core asymmetries on tropical cyclone potential intensity [J]. J Atmos Sci, 2007, 64 (4): 1165-1188.
[36] ZHANG Zhen-yu, WEI Shao-yuan. The introduction of the mesoscale numerical model [J]. J Meteor Sci, 1983, 3 (2): 115-116 (in Chinese).
[37] CHEN De-hui, XUE Ji-shan. An overview on recent progresses of the operational numerical weather prediction models [J]. Acta Meteor Sinica, 2004, 62(5): 623-633 (in Chinese).
[38] LIAO Dong-xian. On the design of the atmospheric model [J]. Acta Meteor Sinica, 1999, 57 (5): 513-524 (in Chinese).

Citation: WEN Ying-fang, LIU Yu-di, TAN Wei-cai, et al. The impact of horizontal resolution on the intensity and microstructure of super typhoon Usagi [J]. J Trop Meteor, 2019, 25(1): 24-33.